Laser Compton scattering photon beams and other X-ray and gamma-ray sources

V.G.Nedorezov

Institute for Nuclear Research RAS, Moscow, Russia

vladimir@cpc.inr.ac.ru

Compton back scattering technique

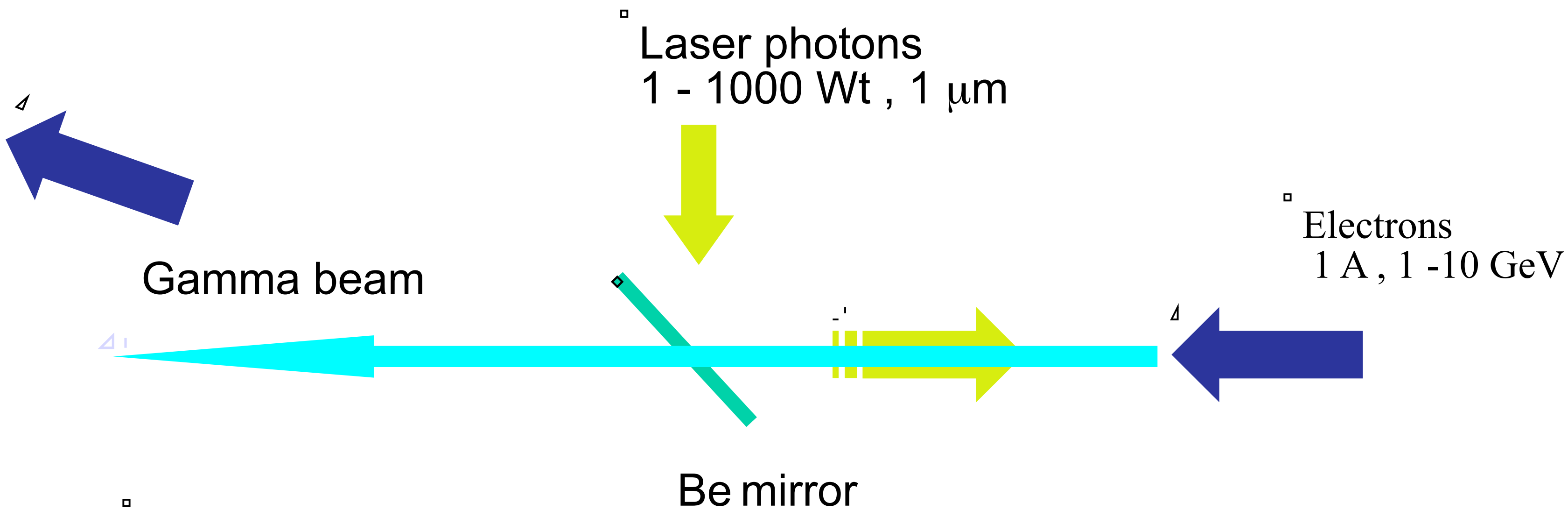

Argon (UV) $N_\gamma < 10^7\ \gamma/s$
CO_2 (IR) $< 10^{10}$
Recirculator $< 10^{15}$

$$E_\gamma = 4\gamma^2 \frac{\omega}{1 + n^2 + \lambda}$$

$n = \theta\gamma$, $\gamma = E_e/m_e$

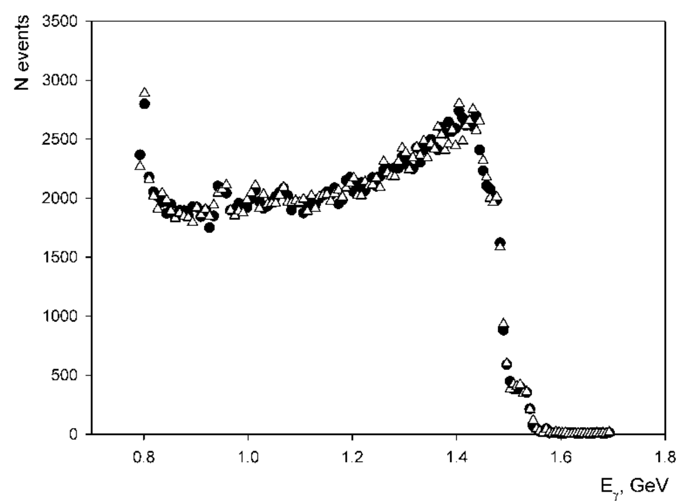

Compton back scattering history

1963 – F.Arutunyan, V.Tumanyan. JETF 44 (1963) 6, 2100.
R.H.Milburn, Phys.Rev.Lett. 10 (1963) 3, 75

1964 – Moscow (Lebedev FIAN) – first experimental evidence

1976 - Frascati (LADONE - ADONE) – photonuclear physics

1984 - Novosibirsk Budker INP (ROKK – 1,2 – VEPP 3,4) meson photoproduction

1988 – Brookhaven BNL (LEGS - NSLS)

1995 – Grenoble (GRAAL – ESRF)

1998 – Osaka (LEPS - Spring-8)

2000 – Duke (HIgS -)

New history: FEMTOSECIND LASER DRIVEN GAMMA SOURCES

QED non-linear effects in photonuclear processes:

Delbruck scattering **Photon splitting** **Coulomb dissociation**

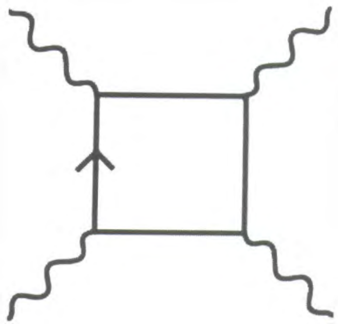

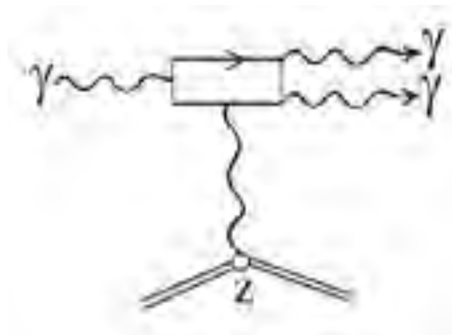

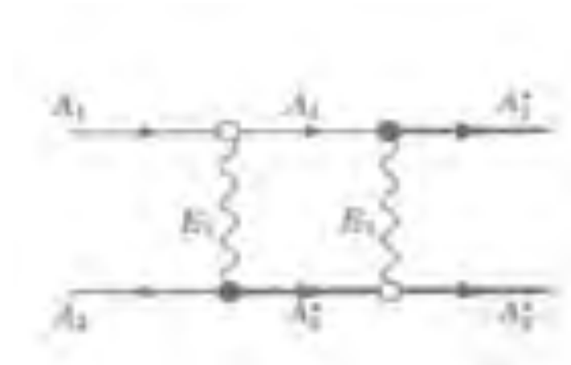

PHYSICS OF STRONG ELECTROMAGNETIC FIELDS:

Photo — and electrofisson of actinide nuclei with low energy and momentum transfer ($Z\alpha \sim 1$)

EM dissociation of relativistic nuclei (maximal EM fields at laboratory conditions)

Femtosecond laser induced photonuclear reactions (relativistic EM field)

Synchrotron radiation at storage rings
Brightness and total intensity

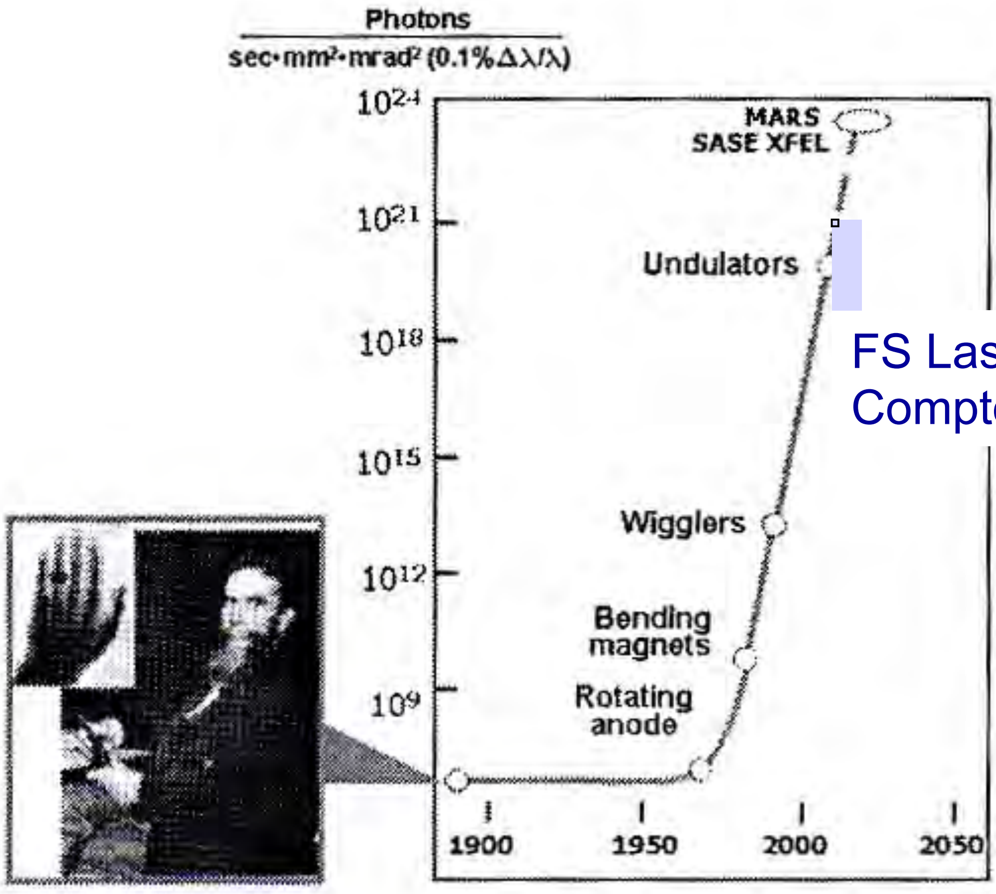

FS Lasers
Compton beams

Relativistic electromagnetic fields produced by femtosecond laser

Mourou G., Tajima T., Bulanov S.V. // Review of Modern Physics. 2006. V.78. P.309-371

Time duration — to 10^{-15} s (femtosecond)

Wave packet length — to 10 μm (10 wave lengths)

Pulse energy - to 100 J, power - to 10^{15} Wt (petawatt).

Focus on radius of 10 μm provides W = 10^{20} Wt/cm^2

Electric field strength E = 10^{12} V/cm

(For comparison: in the hydrogen field E = 10^9 V/см., at mica breakdown - 10^6 V/см Uranium field E = 10^{11} V/cm, with relativistic compression – up to 10^{12} v/cm) .

At E ~10^{11} V/cm, respectively W ~10^{18} Вт/см^2 (λ = 1 μm) electron is accelerated to relativistic velosity being closed to the light one. Therefore such field is defined as the relativistic one .

Nevertheless, direct photonuclear reactions (nuclear excitations) are forbidden.

Quasi-monoenergetic and tunable X-rays from a laser-driven Compton light source N. D. Powers, I. Ghebregziabher, G. Golovin, C. Liu, S. Chen, S. Banerjee, J. Zhang and D. P. Nature photonics letters,

PUBLISHED ONLINE: 24 NOVEMBER 2013 | DOI: 10.1038/NPHOTON.2013.314

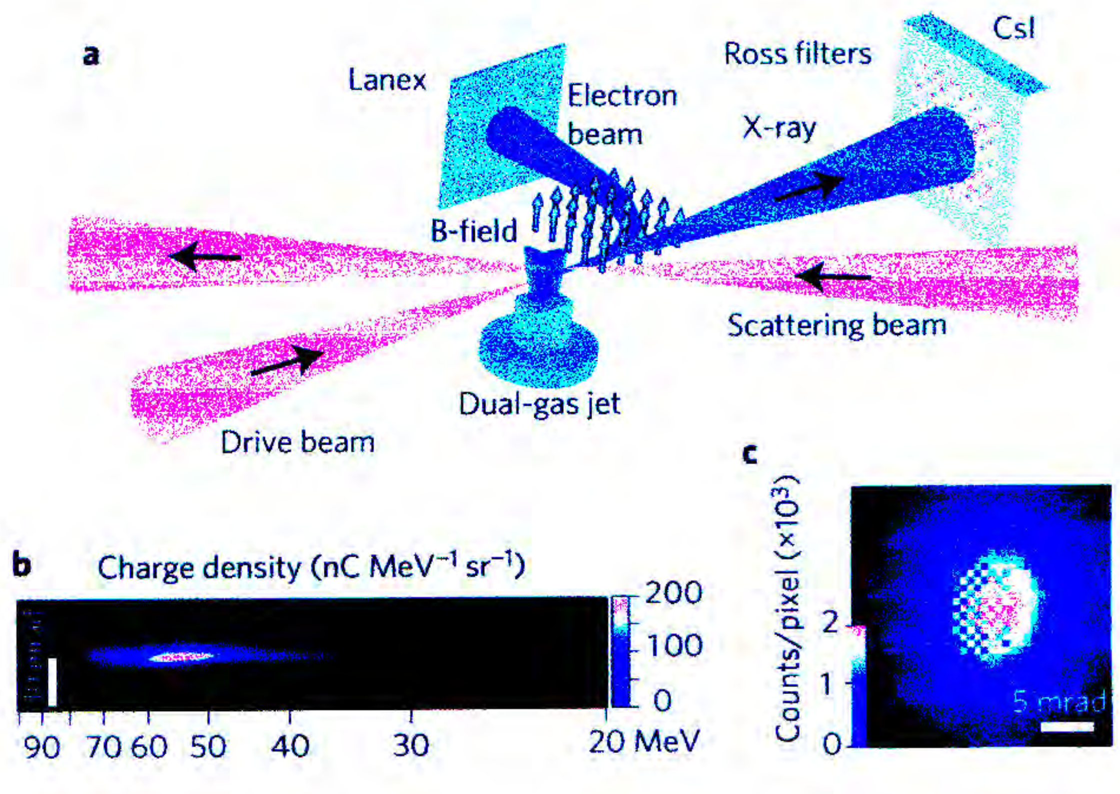

X-ray phase contrast imaging of biological specimens with femtosecond pulses of betatron radiation from a compact laser plasma wakefield (кильватер) accelerator

S. Kneip, C. McGuffey, F. Dollar, M. S. Bloom, V. Chvykov et al.

Appl. Phys. Lett. 99, 093701 (2011)

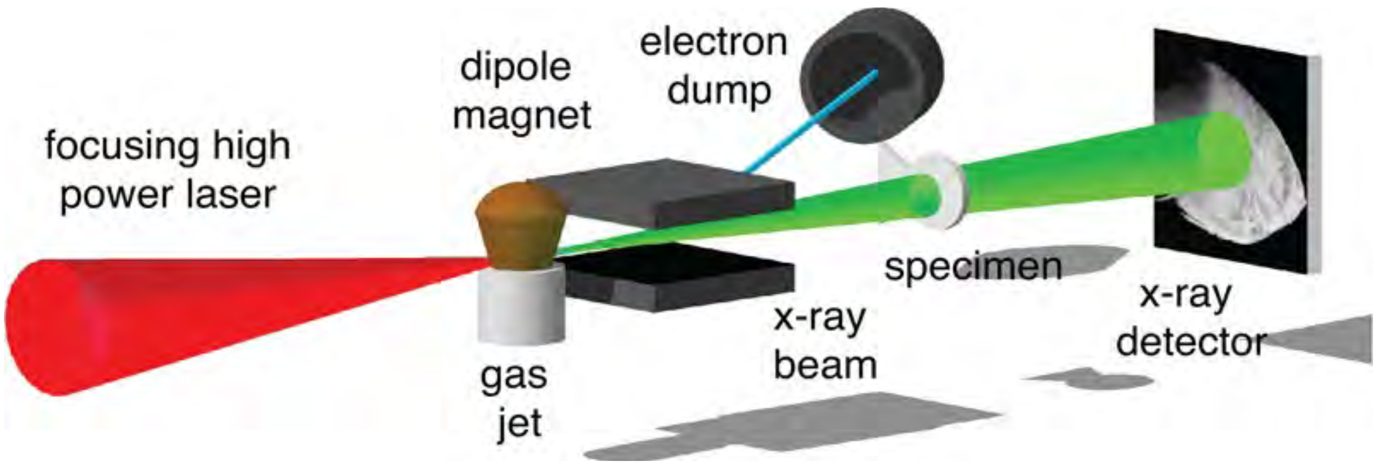

•Hercules laser at the Center for Ultrafast Optical Science at the Uni.of Michigan, Ann Arbor.

•W = 2*10^{19} W/cm^2 (Limit of 10^{20} ; MSU – 2*10^{18}), E = 2 J (MSU - 20mJ)
•fully ionized plasma densities of 3*10^{18} cm^3.
•Electron beams of 100 pC charge and peak energy of 120 MeV (ΔE/E = 3%) - 10^{12} e/имп
•X-ray beam divergence is measured to be 5–15 mrad,
•The x-rays intensity source size as determined with a penumbral imaging technique is found to be 1_3 lm,
•= 10^6 photons/$mrad^2$ from x-ray calorimetry measurements with a ccd camera
•The x-rays spectrum is consistent with a broad synchrotron like spectrum with average photon energy (critical energy) of E_{crit} = 10 keV.
•ultrashort 30 fs burst of x-rays 10 keV, with a peak brightness of 10^{22} ph/s/mm2/mrad2/0.1% bandwidth, comparable to conventional 3rd generation synchrotrons, making possible high contrast imaging in a single shot

Wake field accelerator

High intensity $I_m > 10^{19}$ Wt/cm^2

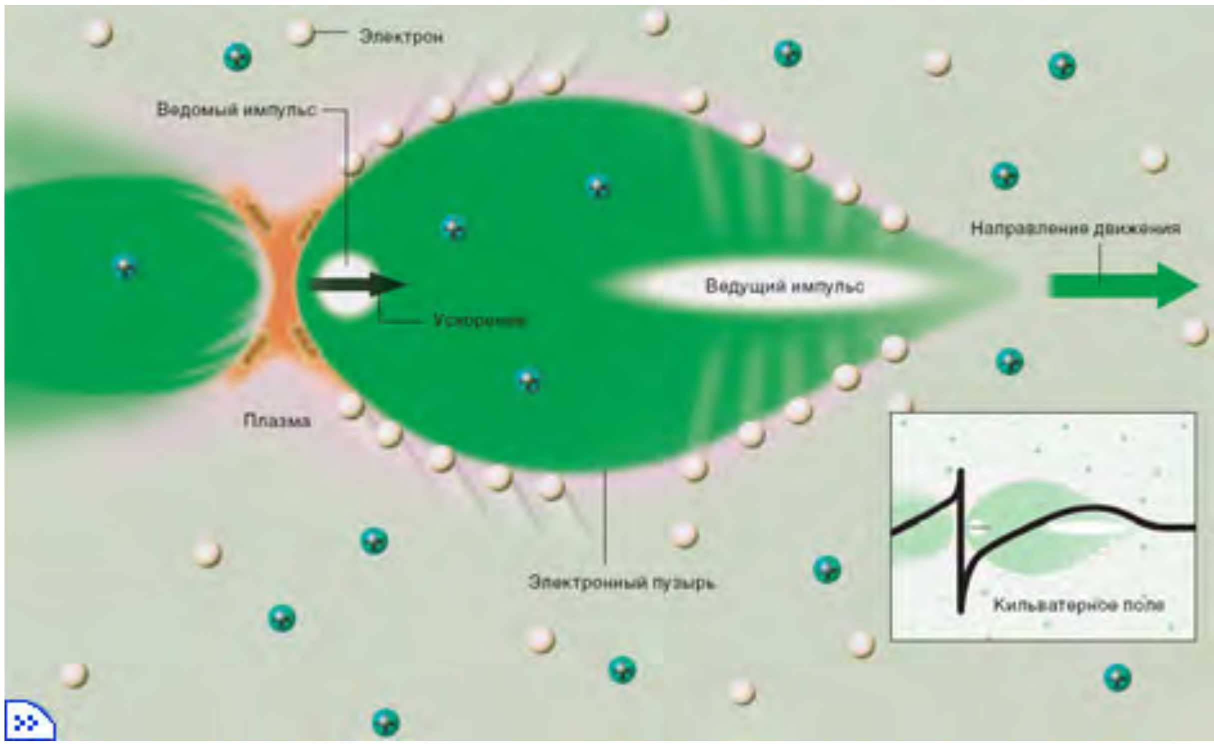

Green area in the center – wake field : leading pulse bubble = positive charge field

Wake accelerating field strength

$$E_0 = cm\omega_p/e$$

Where c – light velocity, e and m- electron charge and mass, ω_p – plasma frequency

Using $\omega_p = (4\pi n e^2/m)^{1/2}$, where n is a plasma density,

$$E_0[\text{В/м}] = 96\, n^{1/2}\, [\text{см}^{-3}]$$

At $n = 10^{18}$ см $^{-3}$, **E_0 = 100 GeV/m**

1) 10^{22} ph/s/mm^2/mrad^2/0.1% bandwidth, 10 mrad, collimation of 4.5 mrad
X-ray phase contrast imaging of biological specimens with femtosecond pulses of betatron radiation from a compact laser plasma wakefield accelerator . S. Kneip, C. McGuffey, F. Dollar, M. S. Bloom, V. Chvykov et al. Appl. Phys. Lett. 99, 093701 (2011)

2) 3×10^{18} photons s^{-1} mm^{-2} mrad^{-2} (per 0.1% bandwidth), 5–15 mrad. Quasi-monoenergetic and tunable X-rays from a laser-driven Compton light source N. D. Powers, I. Ghebregziabher, G. Golovin, C. Liu, S. Chen, S. Banerjee, J. Zhang and D. P. Umstadter* Nature photonics letters (Nov. 2013) p.1-4.

1)

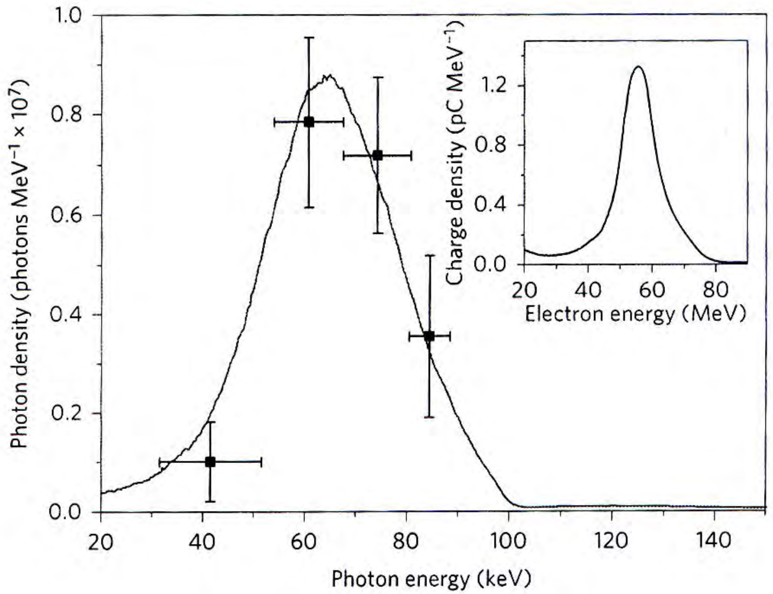

2)

A broad synchrotron like spectrum with average photon energy (critical energy) of Ecrit ’ 10 keV like ESRF.

X-ray phase contrast imaging of biological specimens with femtosecond pulses of betatron radiation from a compact laser plasma wakefield (кильватер) accelerator

S. Kneip, C. McGuffey, F. Dollar, M. S. Bloom, V. Chvykov et al.

Appl. Phys. Lett. 99, 093701 (2011)

- X-ray absorption contrast image of
- a - an orange tetra fish
- b- a damselfly
- [x=2,79 m]

- x-ray phase ontrast image of
- c- a damselfly
- d - a yellow jacket.
- [x = 0,44 m]
- Images are taken with betatron radiation from a laser wakefield accelerator. The spectrum is synchrotron like with E_{crit} ’ 10 keV.
- The phase contrast images are taken in a single shot 30 fs exposure.

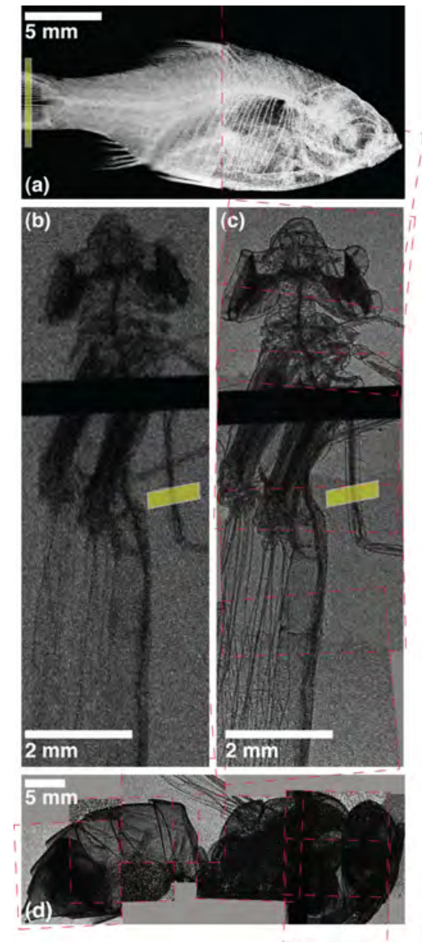

Single shot 30 fs exposure x-ray phase contrast image of the head of a damselfly.
Notice details of the compound eye (1), exoskeleton (2), and leg with hairs (3).

- Each laser pulse delivers
- 30 fs burst of x-rays 10 keV,
- with a peak brightness of 10^{22} ph/s/mm^2/mrad^2 /0.1% bandwidth,
- comparable to conventional 3rd generation synchrotrons, making possible high contrast imaging in a single shot.

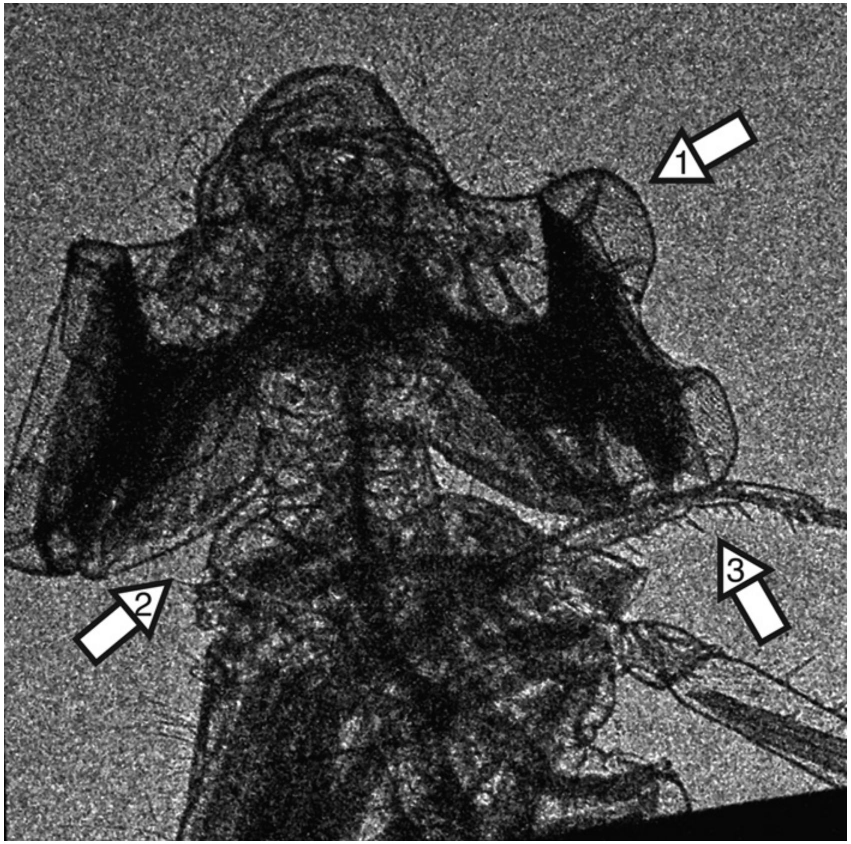

contrast

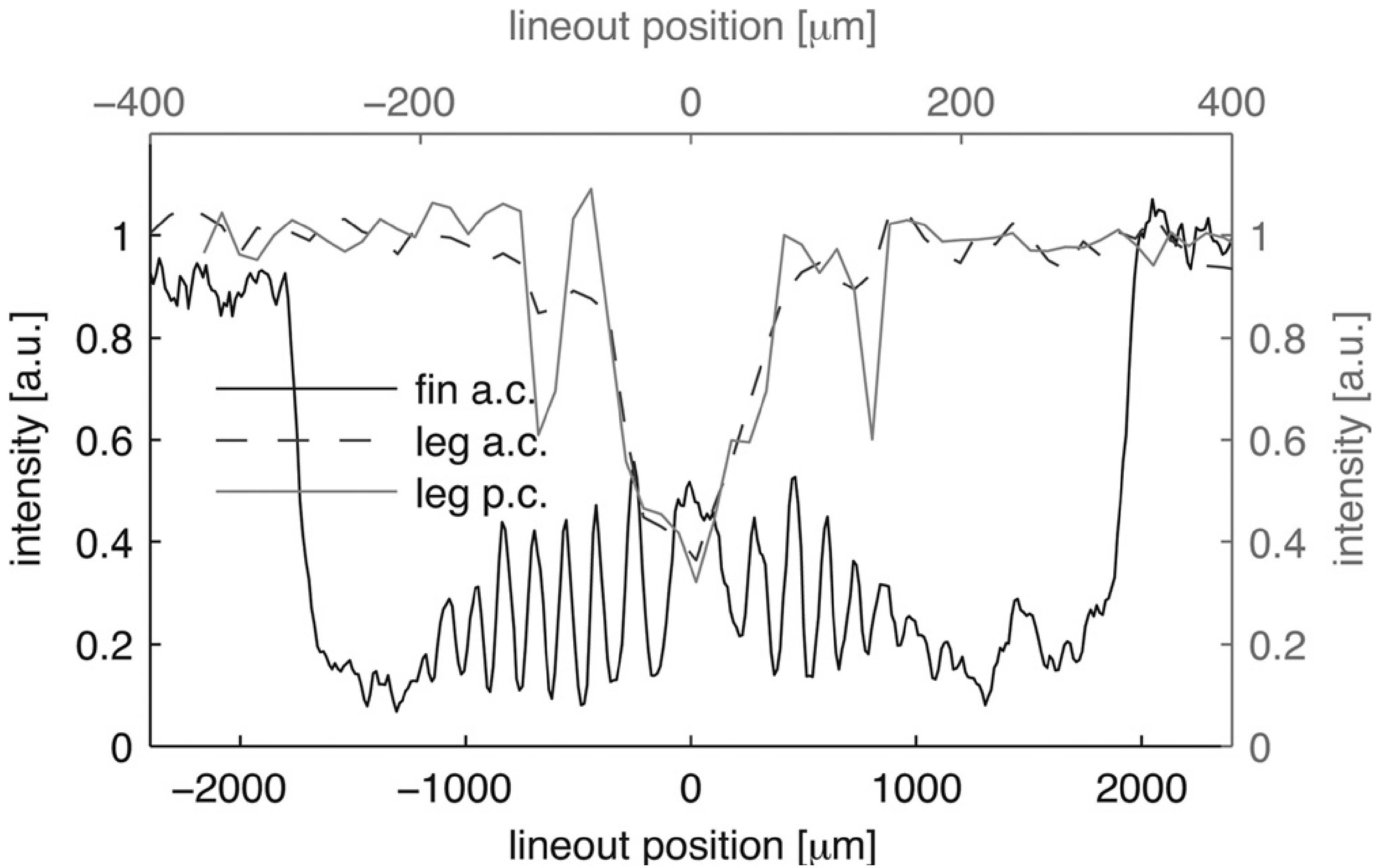

lineout position [μm]
−400
−200
0
200
400
1
0.8
0.6
0.4
0.2
0
intensity [a.u.]
fin a.c.
leg a.c.
leg p.c.
−2000
−1000
0
1000
2000
lineout position [μm]

X-Ray imaging: Three color optics

Medical Applications of Synchrotron Radiation / Eds M. Ando, C. Uyama. Tokyo, 1998

Simultaneously:

Absorption (Ab)
Refraction (An - "Dark field")
Phase contrast (P1,P2),

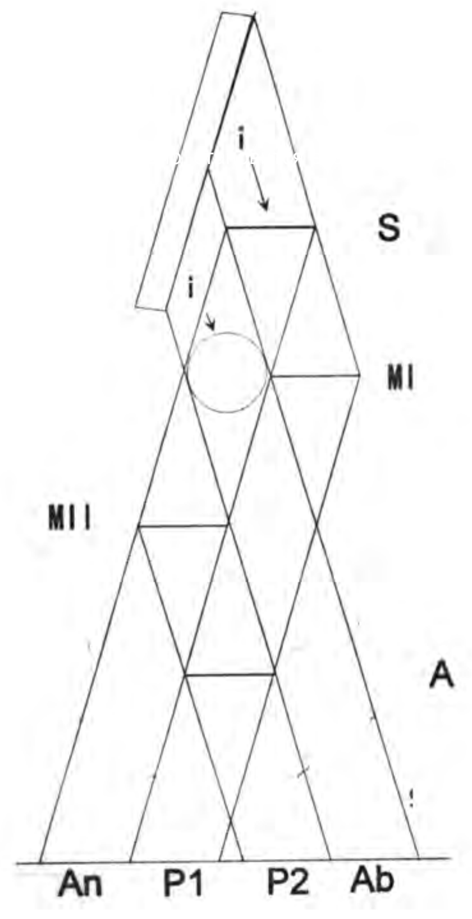

- *S – splitter*
- *MI, MII – mirrors*

Conventional refraction contrast X-Ray diagnostics

1. *Medical Applications of Synchrotron Radiation / Eds M. Ando, C. Uyama. Tokyo, 1998.*
2 S.Shilstein e.a. // Surface:X-ray, synchrotron and neutron researches , 1996, №3, 231-241.

Experimental scheme:

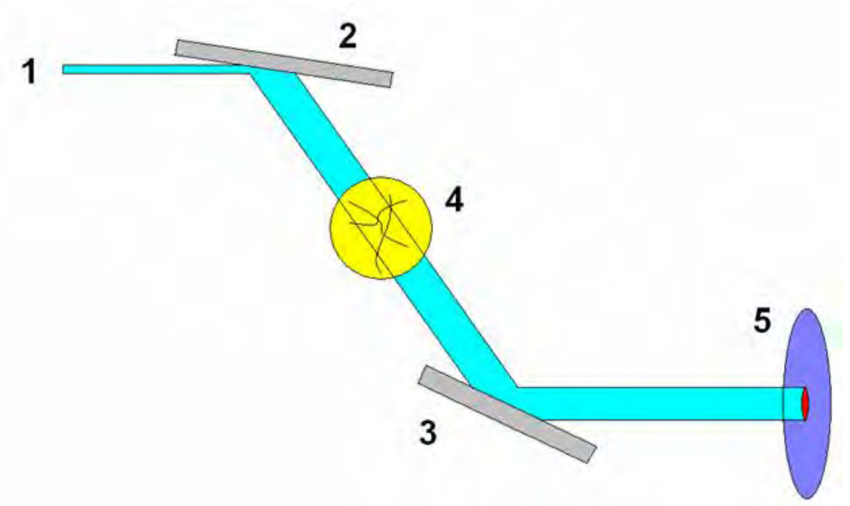

1- synchrotron radiation beam,

2- crystal monochromator,

3- crystal analyzer,

4- object,

5- detector.

Crystal analyser-based X-ray phase contrast imaging in the dark field: implementation and evaluation using excised tissue specimens

M.Ando e.a. European Radiology (2013) ISSN 0938-7994

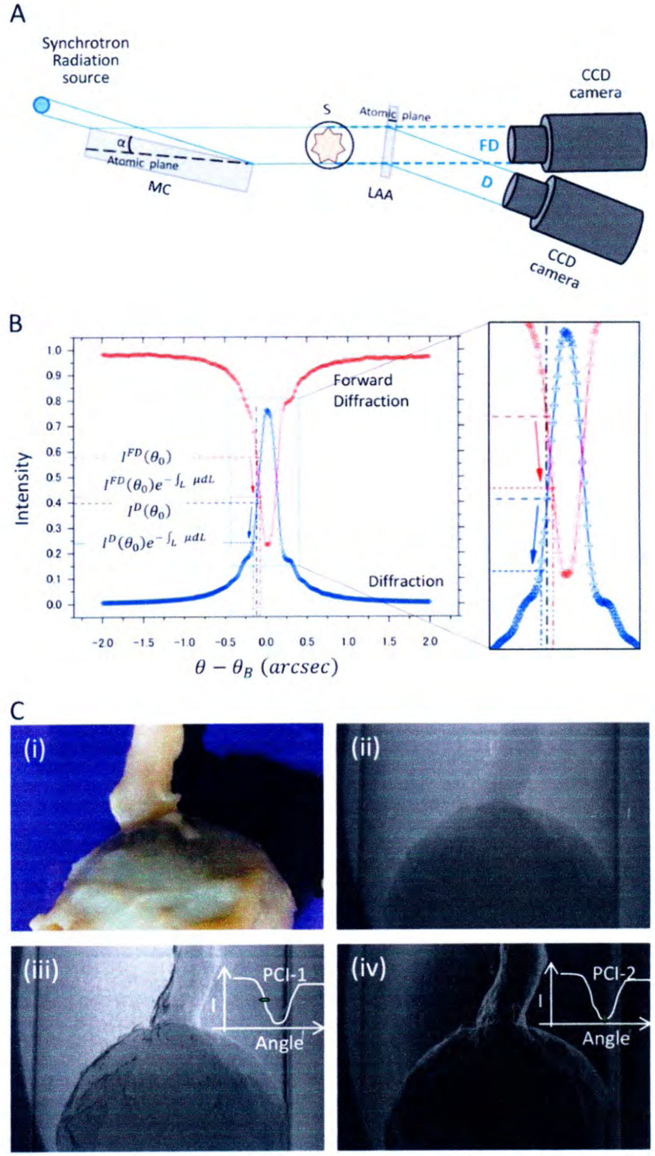

Objectives: the soft tissue discrimination capability of X-ray dark-field imaging (XDFI) using a variety of human tissue specimens.

Methods: The experimental setup for XDFI comprises an X-ray source, an asymmetrically cut Bragg-type monochromator-collimator (MC), a Laue-case angle analyser (LAA) and a CCD camera. The specimen is placed between the MC and the LAA. For the light source, we used the beamline BL14C on a 2.5-GeV storage ring in the KEK Photon Factory, Tsukuba,Japan.

Results: In the eye specimen, phase contrast images from XDFI were able to discriminate soft-tissue structures, such as the iris, separated by aqueous humour on both sides, which have nearly equal absorption. Superiority of XDFI in imaging soft tissue was further demonstrated with a diseased iliac artery containing atherosclerotic plaque and breast samples with benign and malignant tumours. XDFI on breast tumours discriminated between the normal and diseased terminal dictlobular unit and between invasive and in-situ cancer.

Conclusions: X-ray phase, as detected by XDFI, has superior contrast over absorption for soft tissue processes such as atherosclerotic plaque and breast cance

Refraction contrast

Scattering angle on the air – object boundary at geometry optics approximation :

$$\delta\alpha = (1 - n)\cdot \mathrm{ctg}\,\alpha$$

Refraction factor for boundary of organic tissue and air :

$$(1 - n) = 1.5\cdot 10^{-6}\,\lambda^2,$$

Where α — angle between the proton beam and refraction surface, n — *refraction index* , λ — wave length (angstroms).

Image contrast depends on the density gradient, therefore the image has clearly marked sharp boundaries

Refraction imaging of the mammography fantom at KSRS

X-Ray Energy is variable from 10 to 40 keV, Flux is 10^{11} cm^{-2} s^{-1} in the energy bin of 0.1 %. Beam height is variable from 1 to 150 mm, width 150 mm. Angular resolution 0.1 s.

S.Shilstein e.a. Surface, X-ray, synchrotron,, neutron researches. 1996, №3, 231-241.

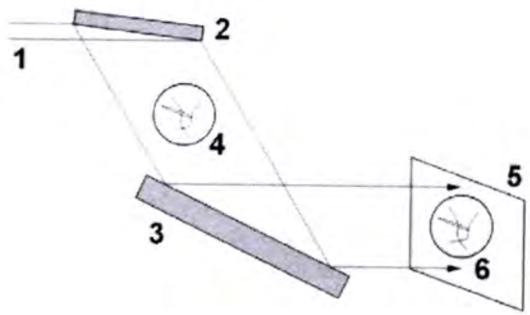

1 – X-ray beam ,
2- monochromator,
3 – analyzer
4 – sample',
5 – detector,
6 - image

Табл.2 Рефракционные изображения фрагментов фантома с частицами Al_2O_3 (модель микрокальцинатов).

размер мм	№ по Рис.3	без корпуса	в корпусе
0.16	10		
0.24	11	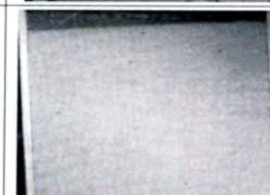	
0.32	12		
0.54	6		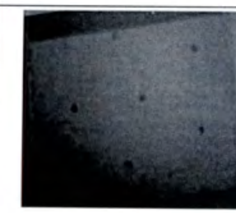

Phantom fragment images (1x1 cm^2), simulating mammography implements (from MEDIANA medical station at KSRS
S.Shilstein e.a. Surface, X-ray, synchrotron,, neutron researches. 1996, №3, 231-241.

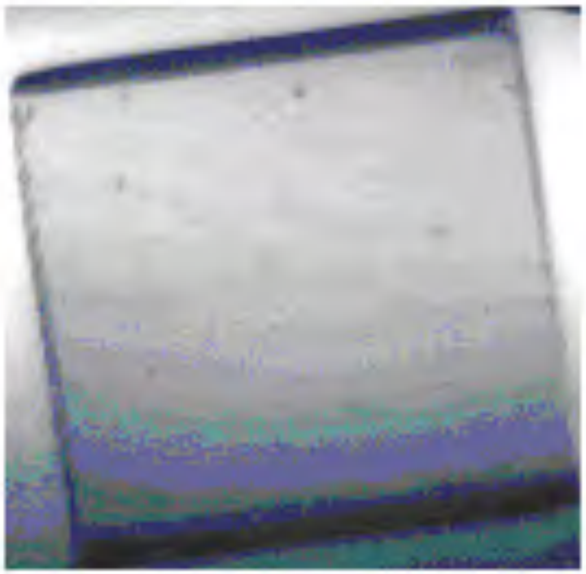

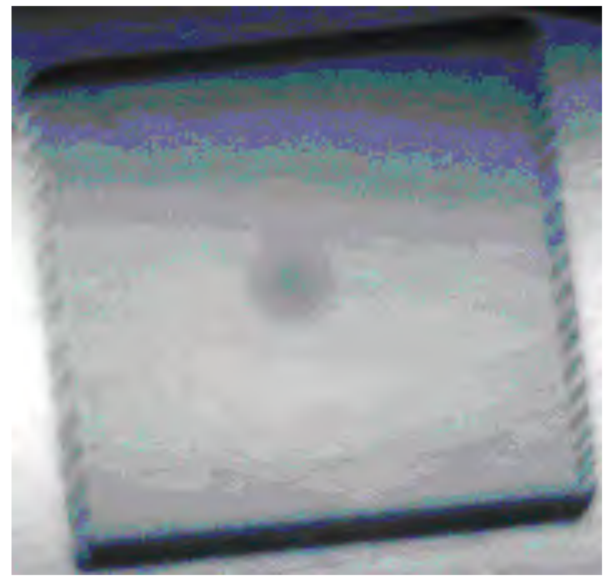

Medical densitometer DENIS

V.G.Nedorezov
Institute for Nuclear Research (INR) RAS, Moscow
S.S.Rodionova,
Central Institute of Traumatology and Orthopaedy (CITO) , Moscow

X-Ray tube

Laser Indicator

Computer

CCD detector
(under the table)

Table

Image of bone with the protez
Medical densitometer DENIS

Calibrator

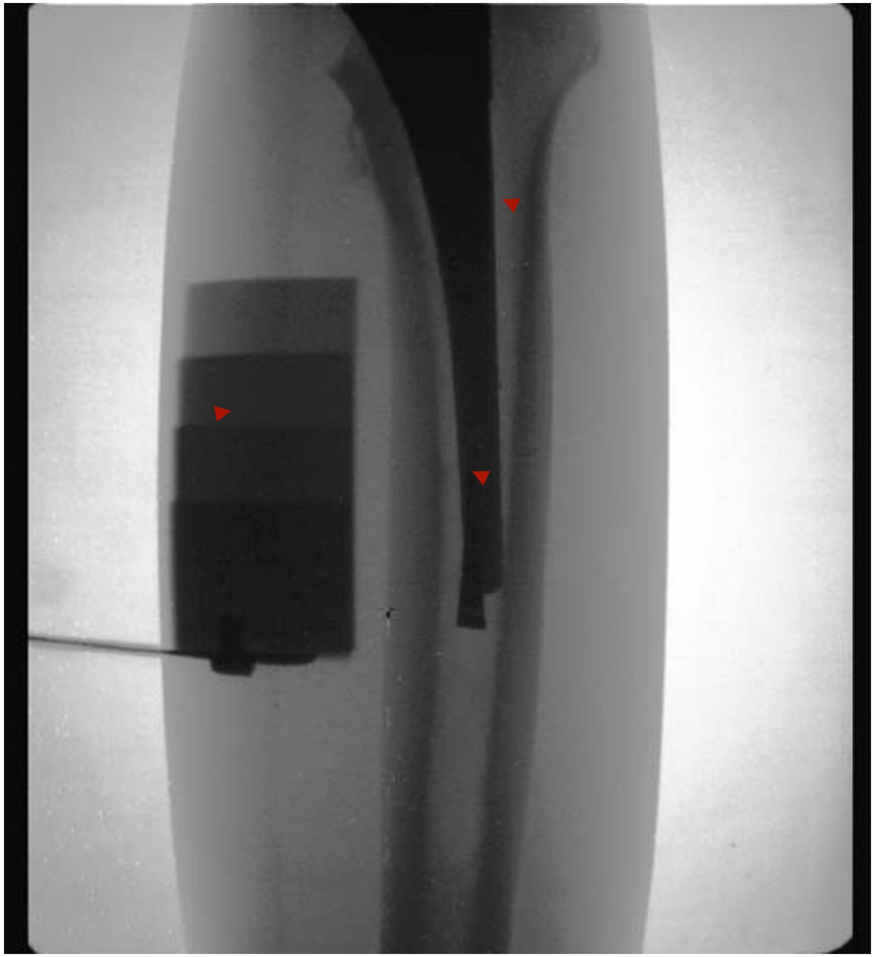

Bone (thigh)

Implantant
(osteo-protez)

AGE FACTOR: bone density dynamics for women of different ages vs time after operation (months)

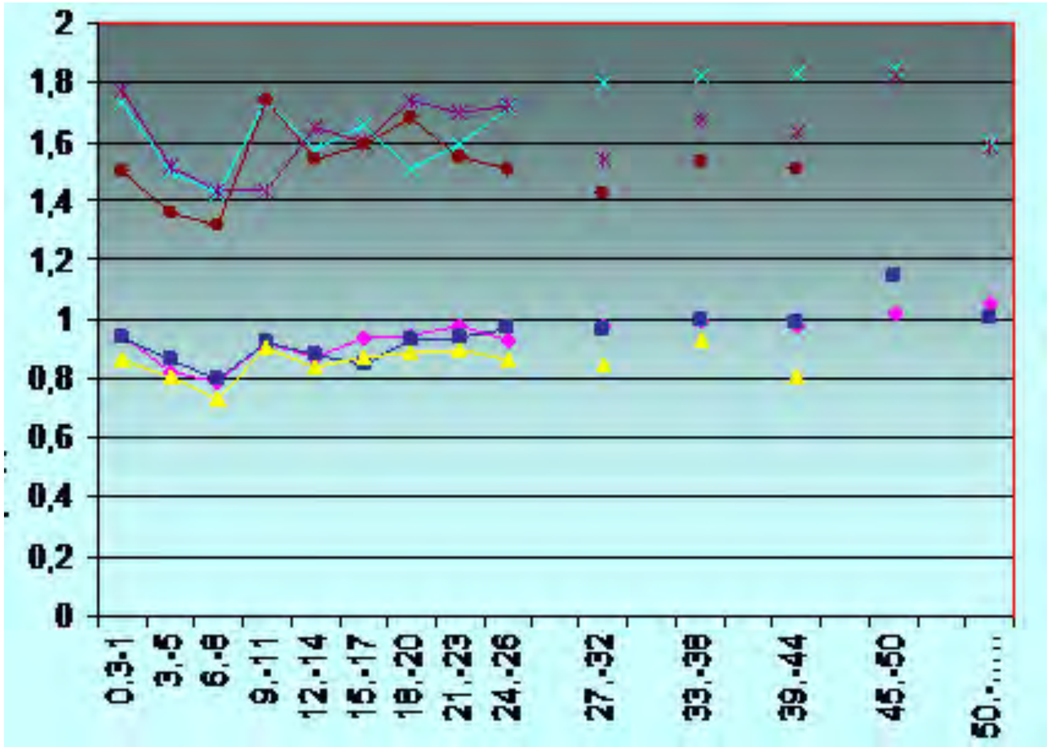

Age (years)	Zone	Color	Zone	Color
< 60	1	red	4	light blue
60 – 70	1	blue	4	lilac
>70	1	yellow	4	burgundy

\

SMOKING FACTOR: bone density dynamics for smoking and non smoking women vs time after operation (months)

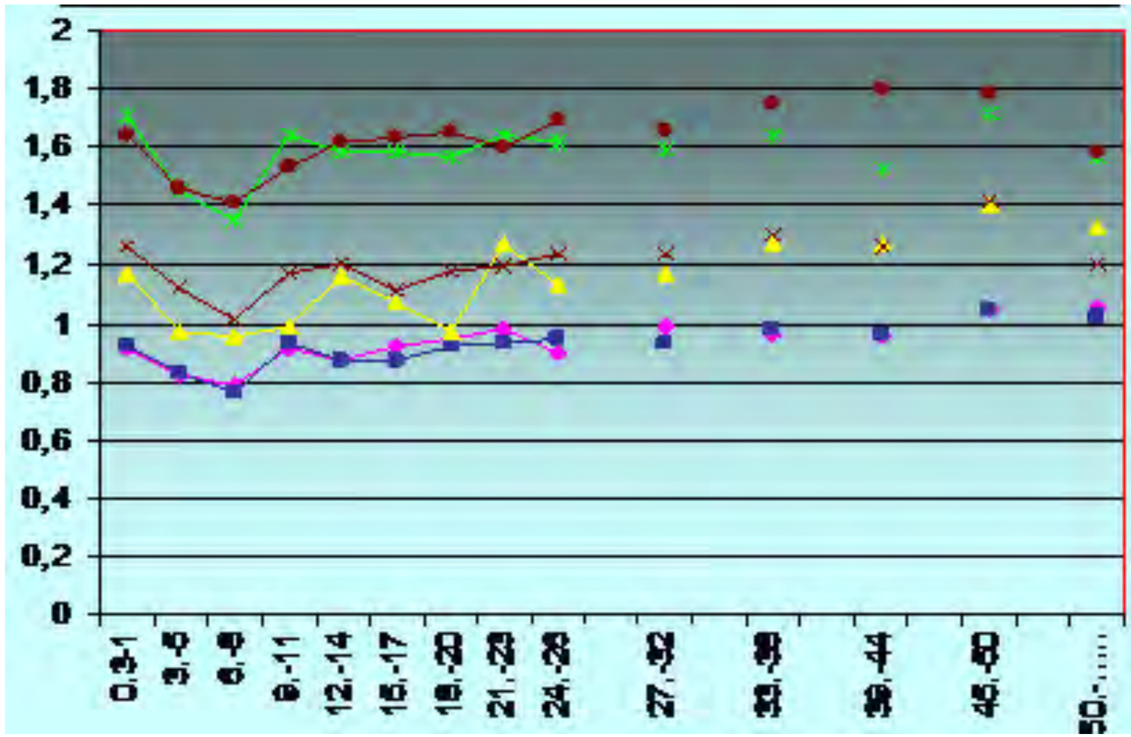

Smoking	Zone	Color	Smoking	Zone	Color
yes	1	red	no	2	light blue
no	1	blue	yes	4	lilac
yes	2	yellow	no	4	burgundy

\

Refraction contrast – bone bioptat

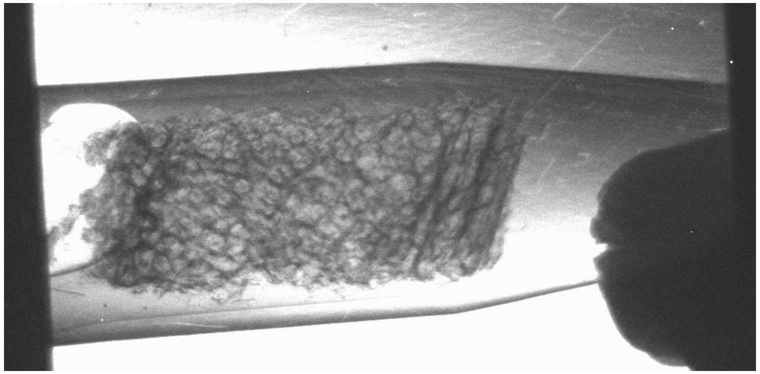

Cortical structure of the bone:

SIgnature of the Osteoporosis

Refraction (upper image) and absorption

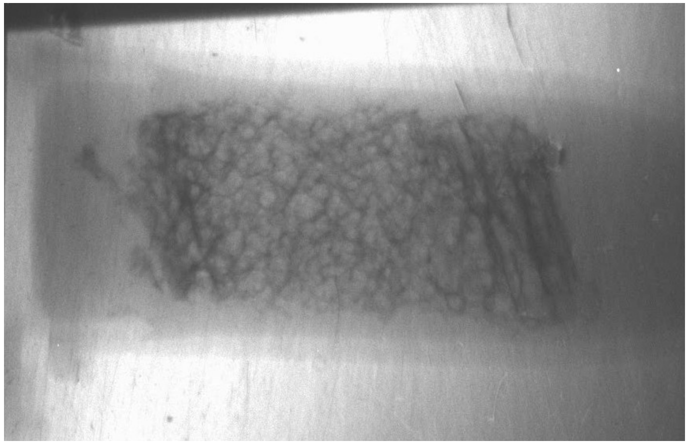

Image contrast and absorbed dose for refraction and absorption diagnostics

Энергия (кэВ)	15	20	30	40	50
Длина волны (А)	0.83	0.62	0.41	0.18	0.14
Число фотонов/мм^2 .сек (x 10^{11})	7.8	3.5	1.1	0.3	0.07
Контраст, % (рефракция)	18	15	11	8	7
Контраст , % (поглощение)	1,3	0,5	0,1	0,06	0,04
Доза, рад (рефракция)	19	1.10^2	4.10^{-4}	2.10^{-4}	2.10^{-4}
Доза, рад (поглощение)	93	0.3	0.1	0.2	0.4

Объект - маммографическиф фантом:

капроновая леска диаметром 1 мм внутри цилиндра воды диаметром 10 см.

FS laser Facilities (2011)

Firm, contry	t,fs	P, 10^{12}Wt	I, 10^{18} Wt/sm^2
1 Lawrence Nat. Lab. (USA)	500	1000	100
2 California Univ. (USA)	30	50	50
3 Michigan Univ. (USA)	30	40	20
4 Texas Univ. (USA)	35	20	0.2
5 Rutherford Lab. (GB)	500	1000	100
6 Astra (GB)	40	40	3
7 ILE (Japan)	500	1000	100
8 AEA (Japan)	30	500	100
9 MBI (Germany)	30	100	10
10 ATLAS (Germany)	100	30	1
11 LULI (France)	30	100	10
12 LOA (France)	30	100	10
13 LUND (Sweden)	30	30	10
14 CIO (China)	500	1000	100
15 NIKI (Russia,Sosnovi Bor)	1000	40	10
16 IPF (Russia, N.Novgorod)	40	560	100
17 MLC MSU (Russia, Moscow)	50	10	2,5
18 TSNIImash (Russia, Korolev)	1500	10	2
19 GOI (Russia, S.Petersburg)	1500	5	1
20 VNIITF (Russia, Chelabinsk)	1500	5	1
21 IOFAN (Russia, Moscow)	40	0.5	1

Experimental setup:
ILC MSU[1] , INR RAS[2], FIAN [3]

Ivanov K.A., Shulyapov S.A., Turinge A.A., Brantov A.V., Uryupina D.S., Volkov R.V., Rusakov A.V., Djilkibaev R.M., Nedorezov V.G.,Bychenkov V.Yu, Savel'ev A.B.
Contributions to Plasma Physics, 53, 2 (2013) 116-12

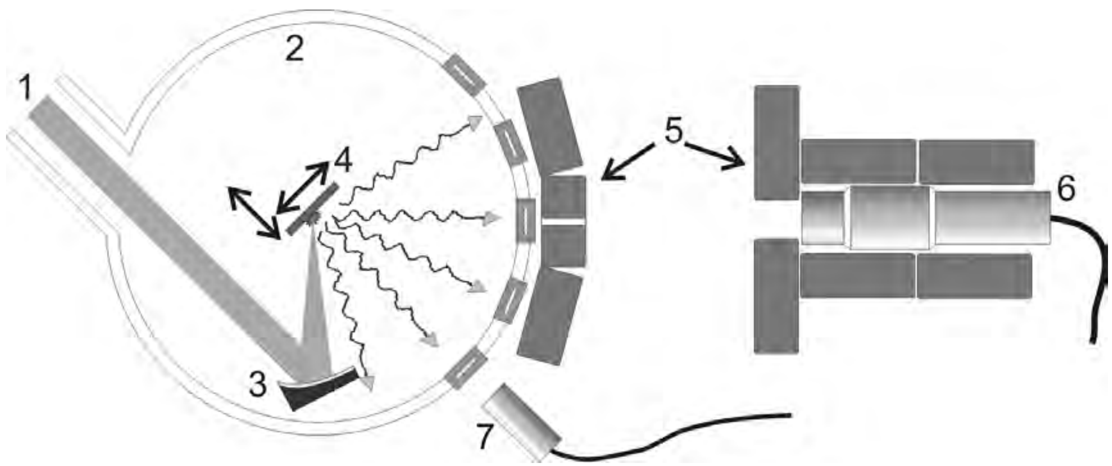

1 – laser radiation, 2 – vacuum chamber, 3 – off-axis parabola, 4 –target on a motorized 3D translation stage, 5 – lead blocks and collimator, 6 – X-ray detector in single quantum regime, 7 – X-ray yield monitor

Laser parameters: 50 fs, 10mJ, 800 nm, 10Hz, peak intensity $2{\cdot}10^{18}$ W/cm^2
contrast on the nanosecond time scale - 2.10^{-6}

Laser facility at ILC MSU

Reaction chamber

Wave length 800 nm,

Impulse length 50 fc,

Frequency 10 Hz,

Pulse energy 50 mJ,

Focusing diameter 4 μm.

Beam intensity on the target 10^{19} W/cm^2,

being equivalent to the electron

quasi-temperature of ~1 MэB.

Runs /03/2013

•FIXED parameters
Laser Ti-Saphire 805 нм , 10 Hz
Target Fe
Contrast - 10^{-8} *
Polarization
Pre-pulse 12.5 ps, 12,5 ns (см.figure)

•VARIABLE parameters :
Energy $5*10^{17}$ - $2*10^{18}$
Duration 45 – 170 fs
Filters Cu 0.5 – 3.6 мм Cu2 мм , Pb 6 mm,
Shield Pb 50 mm

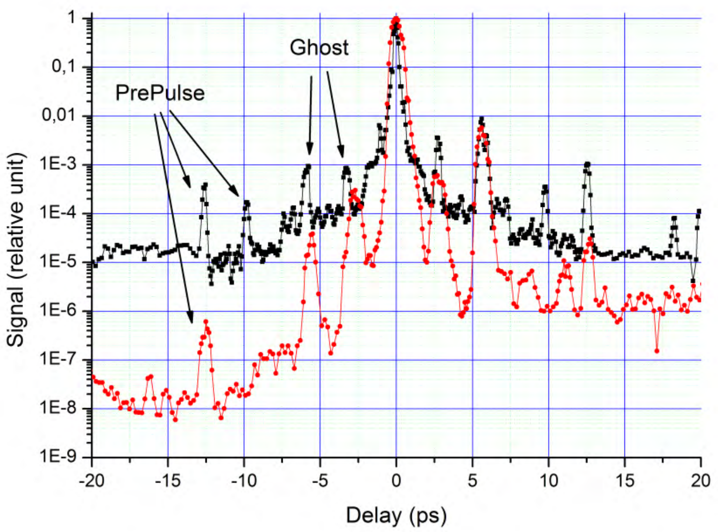

Correlation function
(2012 – black, 2013 – red).

A. Turinge , A. Rusakov, A. Savel’ev, A. Brantov, V. Bychenkov.
Simulation of bremsstrahlung
from interaction of a femtosecond terawatt laser pulses with matter
Proc.EMIN-2012,167- 171

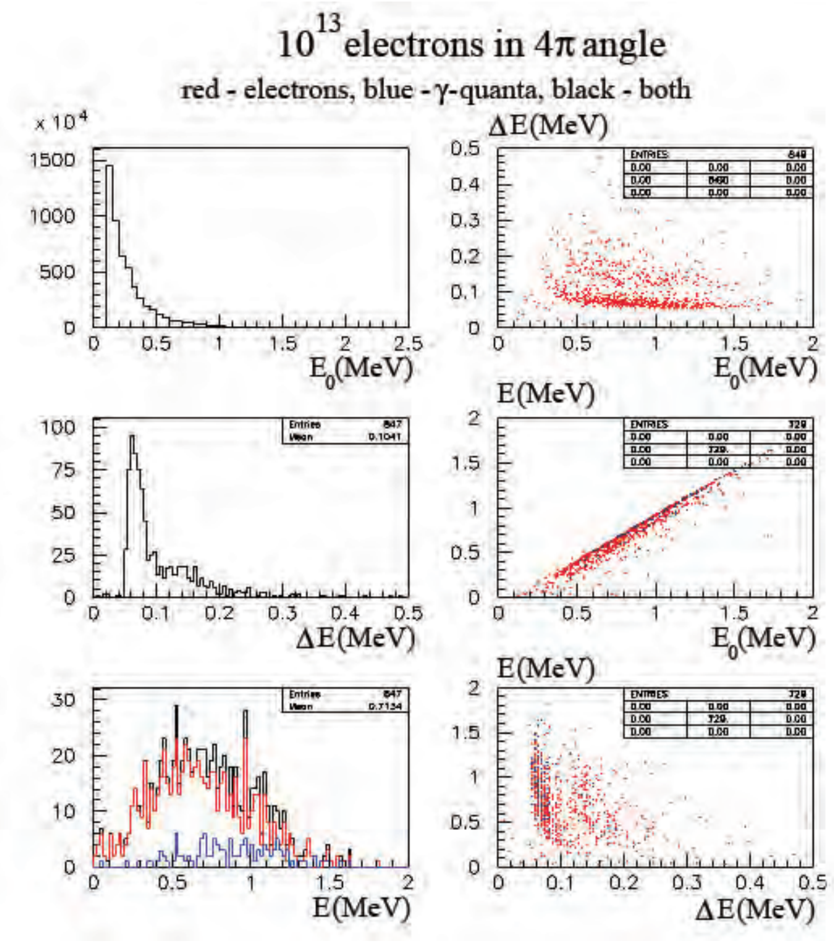

First preliminary experimental results:
ΔE-E spectra for electrons and gammas with energy up to 2.5 MeV

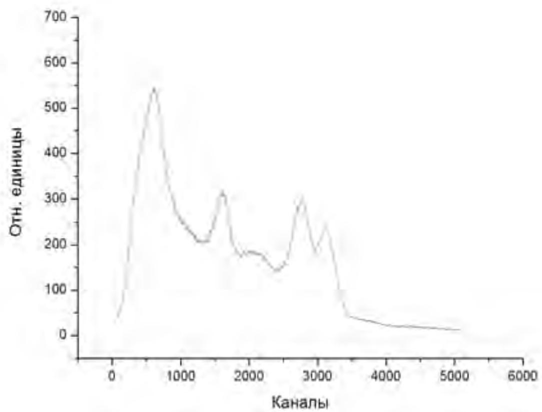

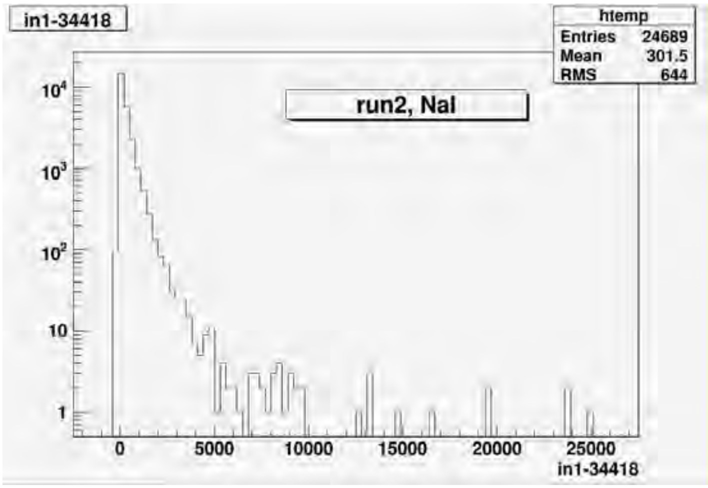

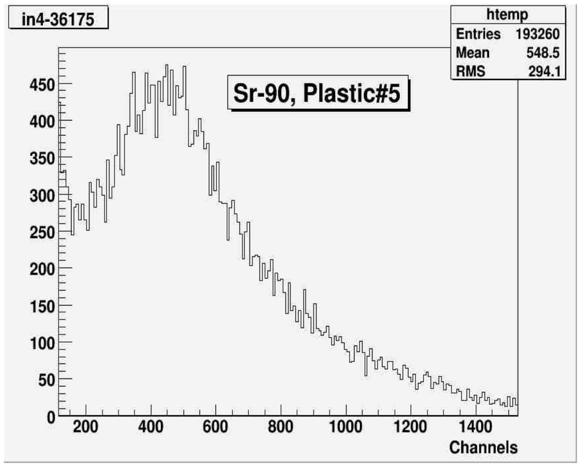

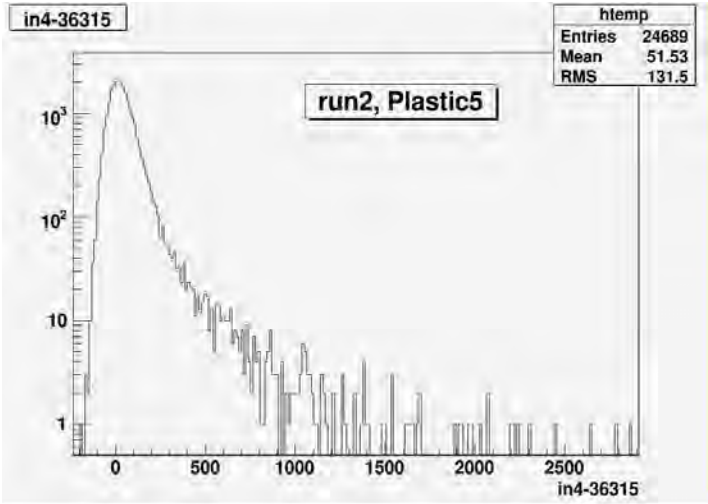

Photon spectra at different conditions

21.03.2013

run 3 : Target – Fe, E = 19.5 mJ, t = 45 fs.
run 4 : Target – Cu

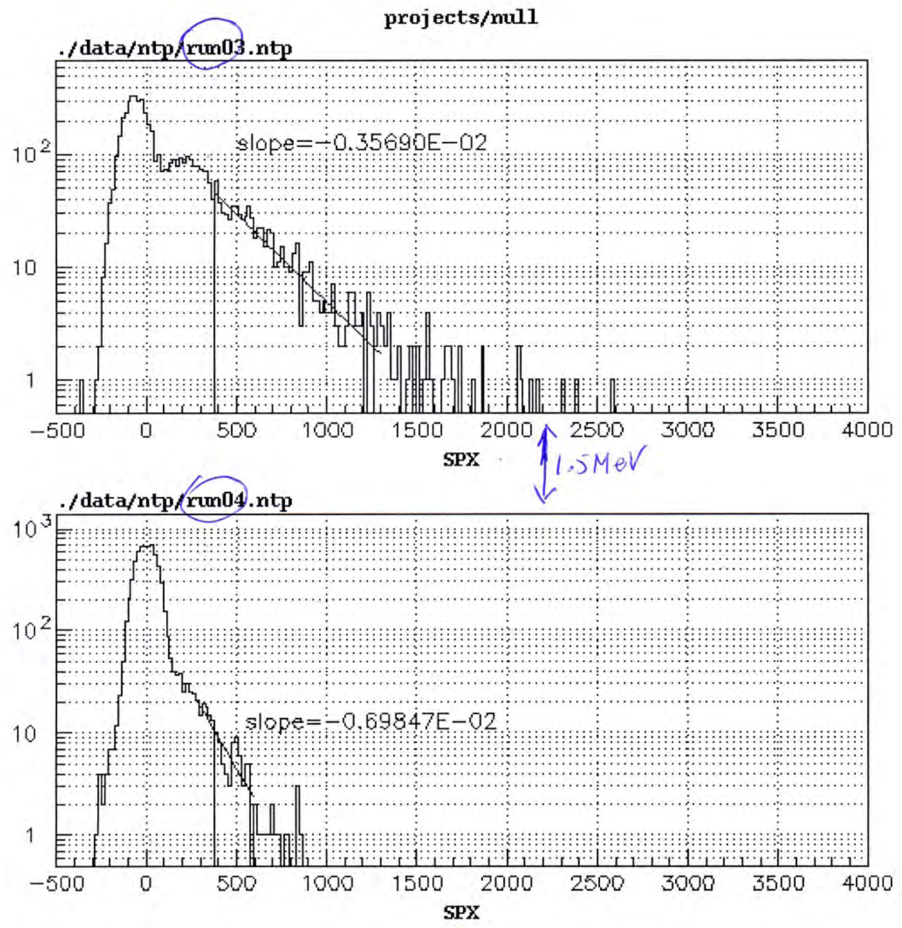

Dependence of photon spectrum on the laser pulse length
filter Cu 3.6 мм Single photon regime

A.V.Rusakov
Study of electromagnetic radiation from the iron target, irradiated by femtosecond laser pulses , NUCLEUS -2013, Friday, Section V, Mephi, Moscow

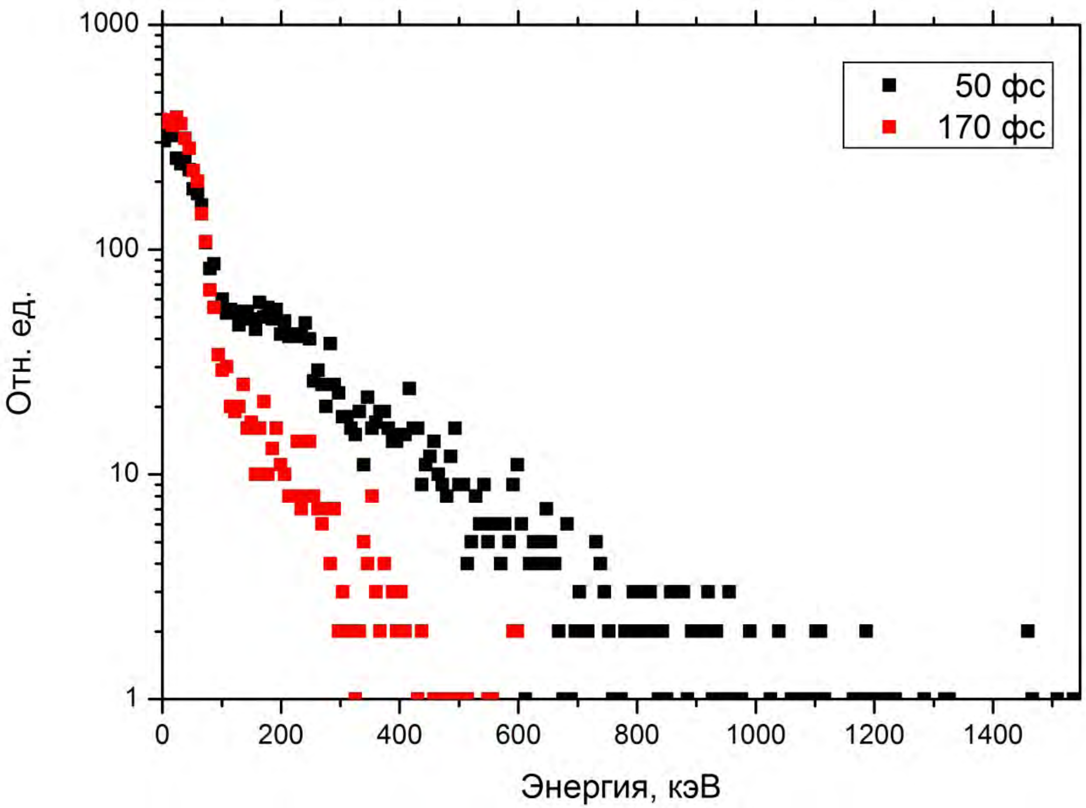

Dependence of photon spectrum on pulse energy , filter Cu 3.6 mm

A.V.Rusakov

Study of electromagnetic radiation from the iron target, irradiated by femtosecond laser pulses , Friday, Section V

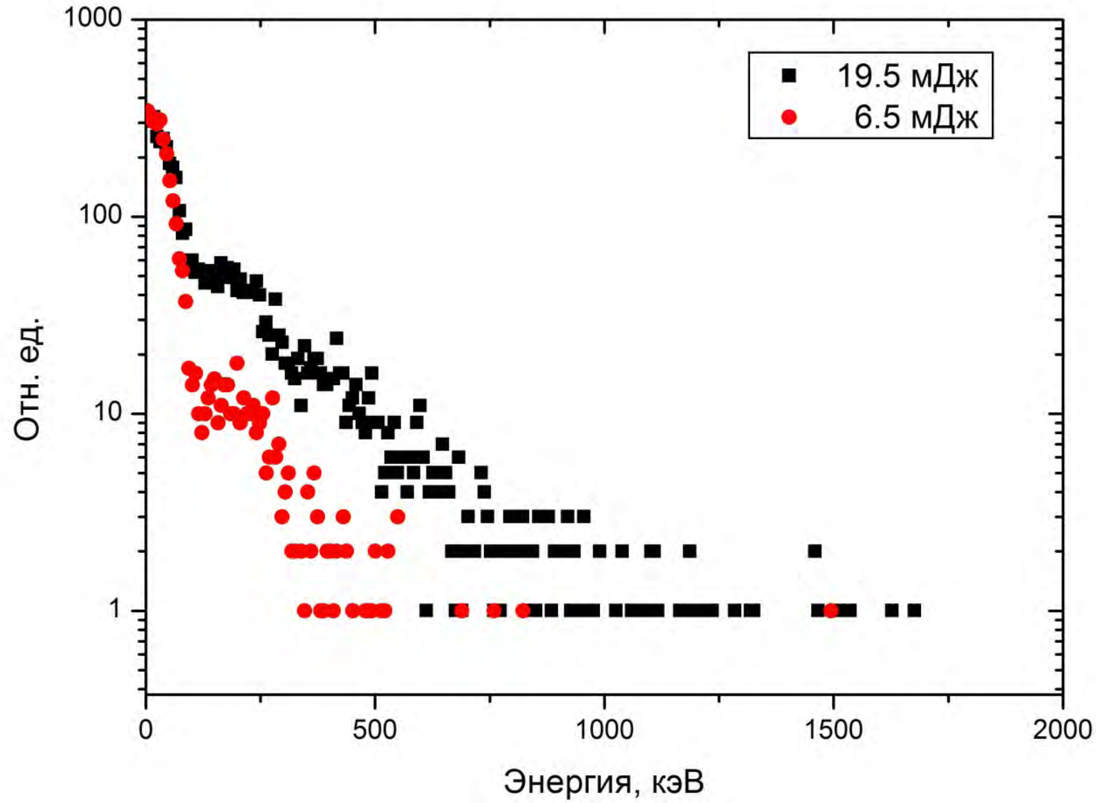

Experiment and simulations
Single photon regime

Squares – photon energy spectrum (experimental results) ;

Below: Backgrounds from lead blocks, chamber walls etc.)

Straight lines – approximation (slope of two exponents)

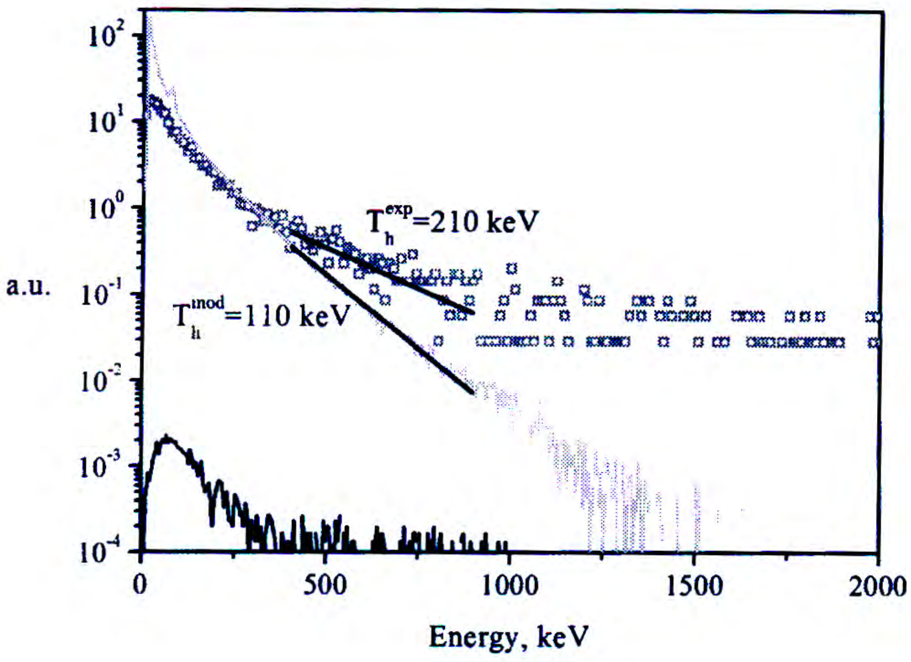

Mechanisms of femtosecond laser electron acceleration at low intensity

A.V.Andreev, V.M.Gordienko, A.B.Savel'ev. "Nuclear processes in the high temperature plasma induced by the super short laser pulse" Quantum electronics 31,11 (2001) 941-956.

"At energy concentration of 10^{11} J/cm^3 the energy transfer to separated **atom** can exceed 10 MeV while the binding energy for **nucleon** is near 8 MeV".

High temperature electron production mechanisms (atomic processes) at relatively low intensity $I_m < 10^{17}$ Wt/cm^2 :

- Resonance absorption, $\lambda/L > 1$
- Vacuum heat, $\lambda L < 1$
- Anomalous skin-effect $\lambda L << 1$

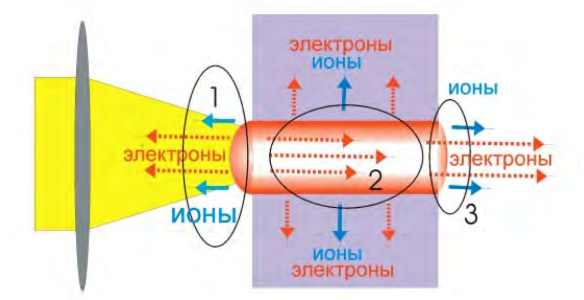

$$L = (d\ln N_e/dz)^{-1}$$

Future close tasks for ILC MSU team

New experimental results and systematization:
photon spectra at different parameters.

Diagnostics of products in the separated laser shot :
electron spectrometer inside the vacuum chamber

Electron magnetic spectrometer project

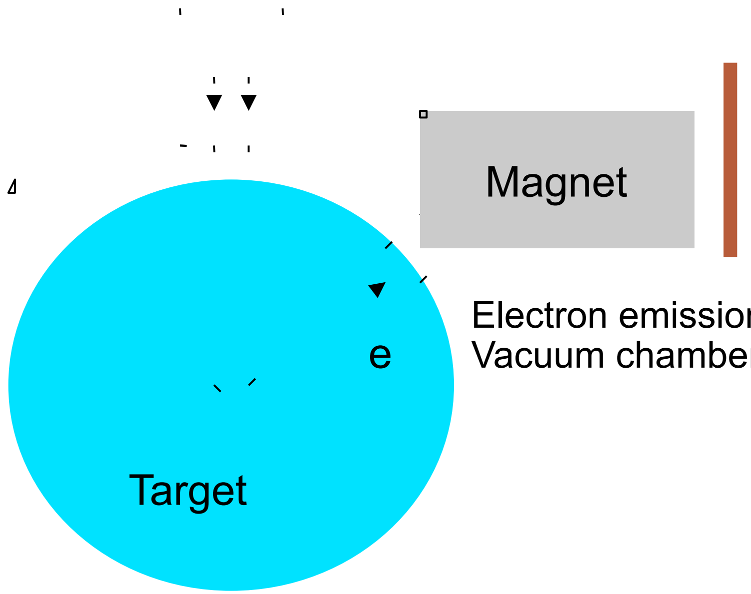

Coordinate detector in the focal plane
1 mm resolution

Electron emission angle fixed
Vacuum chamber diameter 40 cm

Radiation point 10 x 10 μc diameter
Electron energy of 10 keV till 50 MeV.
Electron pulse flux to 10^6 ./s , frequency 10 Hz

Energy ranges for 1% resolution : 100 — 1000 keV, 1 — 10 MeV, 10 — 50 MeV.

Other gamma ray sources :
Ground-based observations of thunderstorm-correlated fluxes of high-energy electrons, gamma rays, and neutrons

A. Chilingarian e.a. PHYSICAL REVIEW D 82, 043009 (2010)

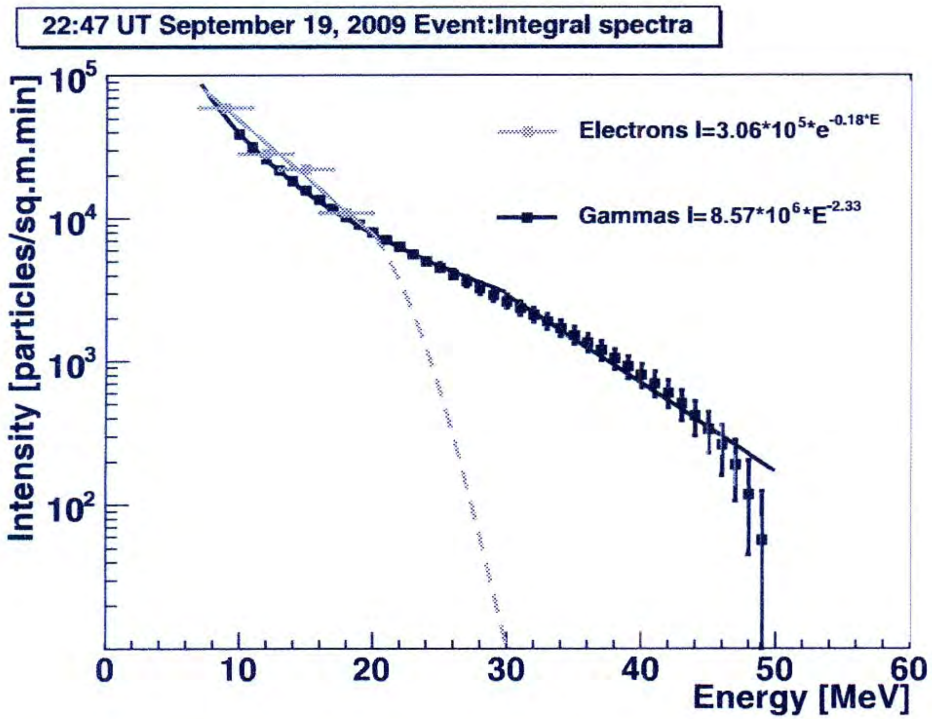

FIG. 7. Unfolded electron and gamma ray spectra fitted by exponential and power functions.

Первые лабораторные наблюдения нейтронных вспышек в разрядах (с кристаллическими дейтерированными мишенями)

PRL **111,** 115003 (2013) PHYSICAL REVIEW LETTERS week ending 13 SEPTEMBER 2013

Observation of Neutron Bursts Produced by Laboratory High-Voltage Atmospheric Discharge

A. V. Agafonov,[1] A. V. Bagulya,[1] O. D. Dalkarov,[1,2] M. A. Negodaev,[1] A. V. Oginov,[1,*] A. S. Rusetskiy,[1] V. A. Ryabov,[1] and K. V. Shpakov[1]

[1]*P.N. Lebedev Physical Institute of the Russian Academy of Sciences (FIAN), Leninsky Prospekt, 53, Moscow 119991, Russia*

[2]*Centre for Fundamental Research (MIEM NRU HSE), Myasnizkaya, 20, Moscow 101000, Russia*

(Received 10 April 2013; published 12 September 2013)

For the first time the emission of neutron bursts in the process of high-voltage discharge in air was observed. Experiments were carried out at an average electric field strength of $\sim 1\ \mathrm{MV \cdot m^{-1}}$ and discharge current of ~ 10 kA. Two independent methods (CR-39 track detectors and plastic scintillation detectors) registered neutrons within the range from thermal energies up to energies above 10 MeV and with an average flux density of $\gtrsim 10^6\ \mathrm{cm^{-2}}$ per shot inside the discharge zone. Neutron generation occurs at the initial phase of the discharge and correlates with x-ray generation. The data obtained allow us to assume that during the discharge fast neutrons are mainly produced.

J.Sentoku, V.Y.Bychenkov e.a. High energy ion generation in interaction of short laser pulse with high density plasma Appl.Phys.B 74 (2002) 207-216.

Gamma and neutron sources

Isotope production

Nuclear physics and photonuclear reactions

Relativistic Ion beams

Astrophysics simulations

Hadron therapy

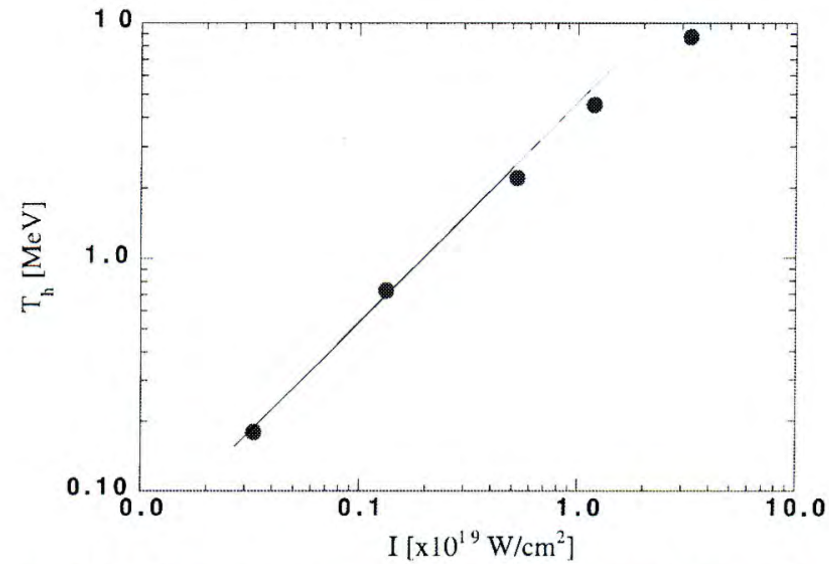

FIGURE 6 Hot-electron temperature at the solid plasma surface versus the laser intensity at 80 fs

Non equilibrium plasma temperature ?

Solar temperature is less than 10 keV;

Respectively - 13,5 * 10^6 degree

Nuclear processes in high temperature plasma, induced by super short laser pulse

A.Andreev, V.Gordienko, A.Saveljev. Quantum electronics 31,11. 2001, 941-956

Electron beams energy exceeds 1 GeV , proton and ion beams energy - 50 MeV per nucleon.

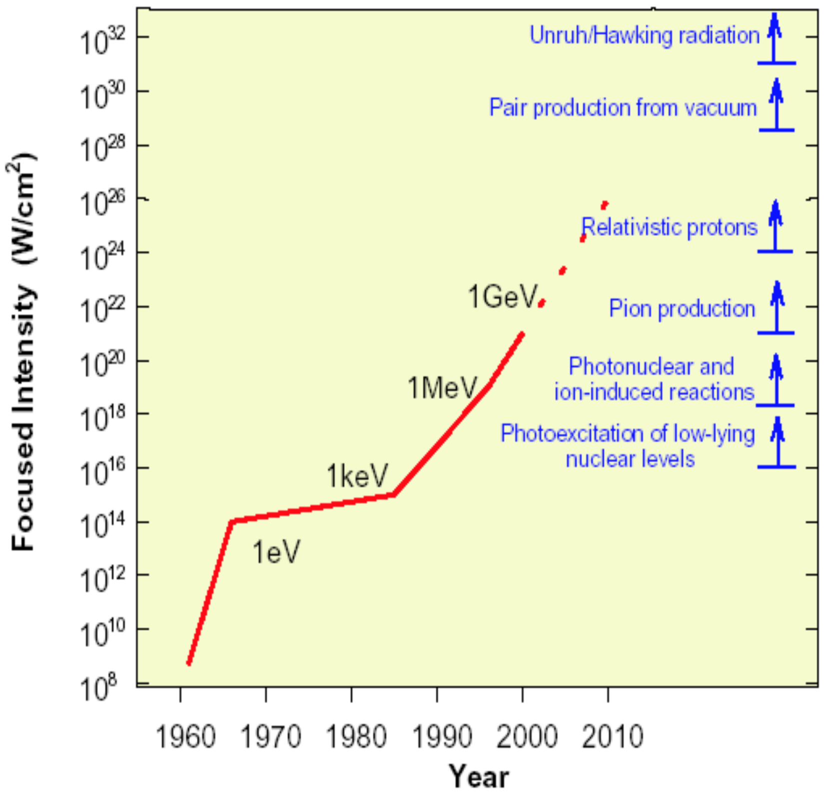

Nuclear processes in high temperature plasma, induced by super short laser pulse

A.Andreev, V.Gordienko, A.Saveljev. Quantum electronics 31,11. 2001, 941-956

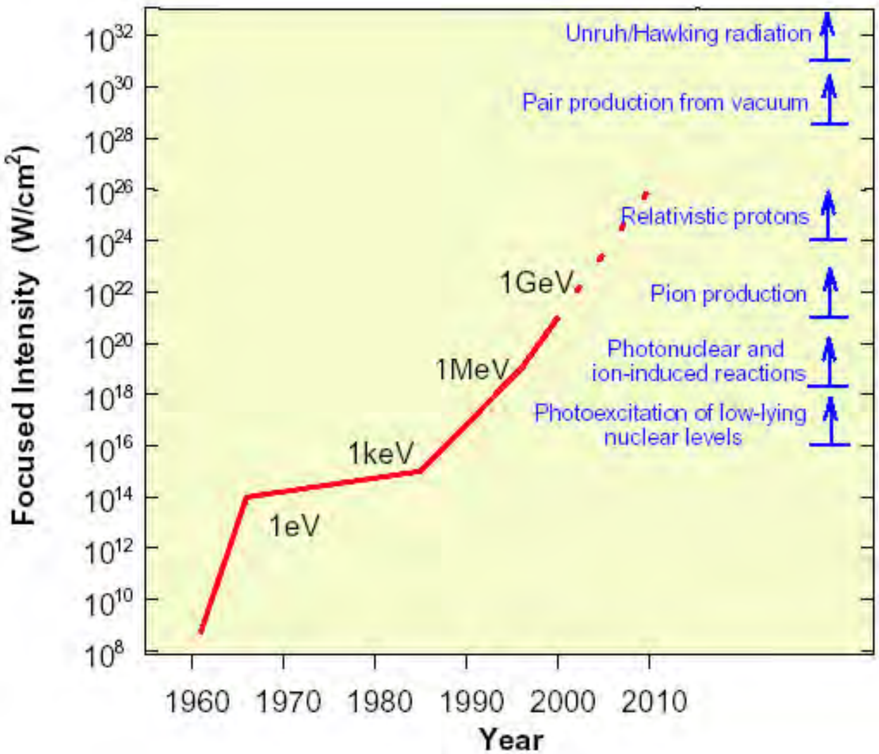

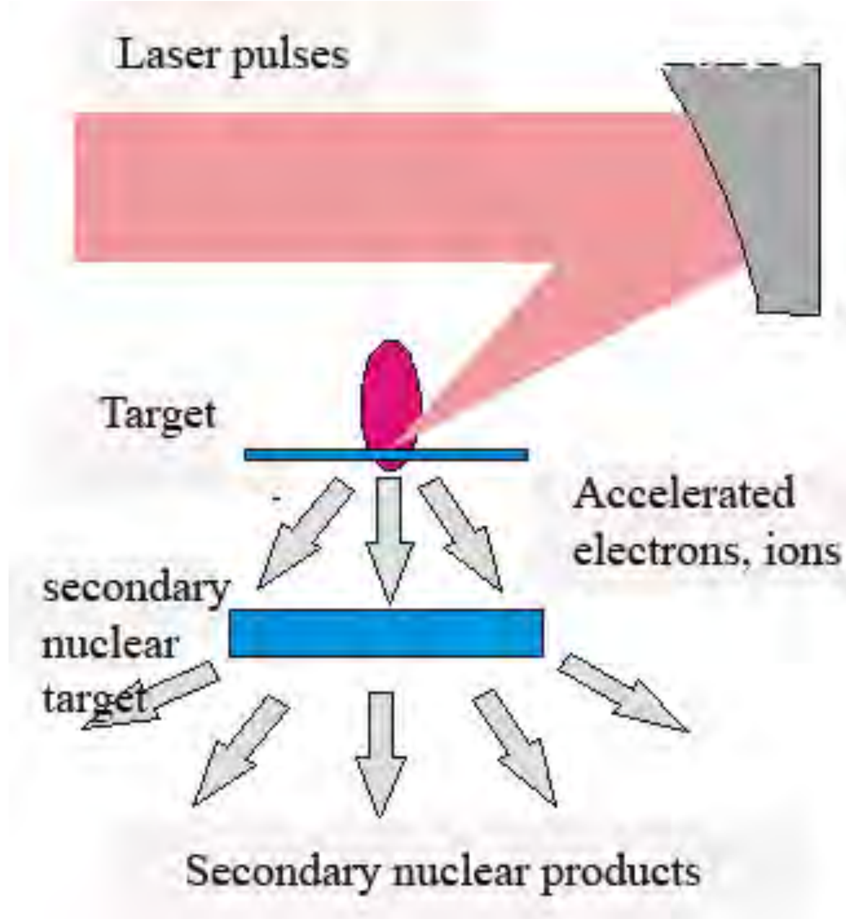

***Photonuclear view**: linear QED*

Compton photon scattering amplitude, dispersion relations

$f = \mathbf{e'^{*}e}\, f_1(w) + i\, w\sigma\, \mathbf{e'^{*}} \times \mathbf{e}\, f_2(w)$

e – EM field calibration invariant operator ,

σ ***– nucleon spin operator***.

At **w = 0** (low energy theorem):

$f1(0) = -\ (\mathbf{a} / \mathbf{Z^2} / \mathbf{M}),\quad f2(0) = (\mathbf{a\ k^2 / 2M^2}),$

M *– mass,* **a = e² /4π** = 1/137

eZ *– electric charge* ,

k *- nucleon anomalous magnetic moment*

$f_1(0) = -(\alpha / Z^2 / M) + \omega^2/2\pi^2\ \sigma_{tot}(w')/f(\omega')\, d\omega'$

$f2(0) = (\alpha\, k^2 / 2M^2) + \omega^2/2\pi^2\ \Delta\sigma_{tot}(\omega')/\phi(\omega')\, d\omega'/\omega'$

Total photoabsorption cross section

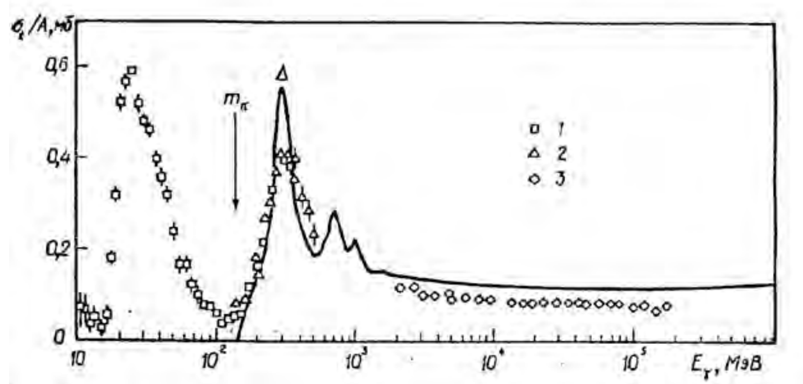

$E_\gamma = hc/\lambda$

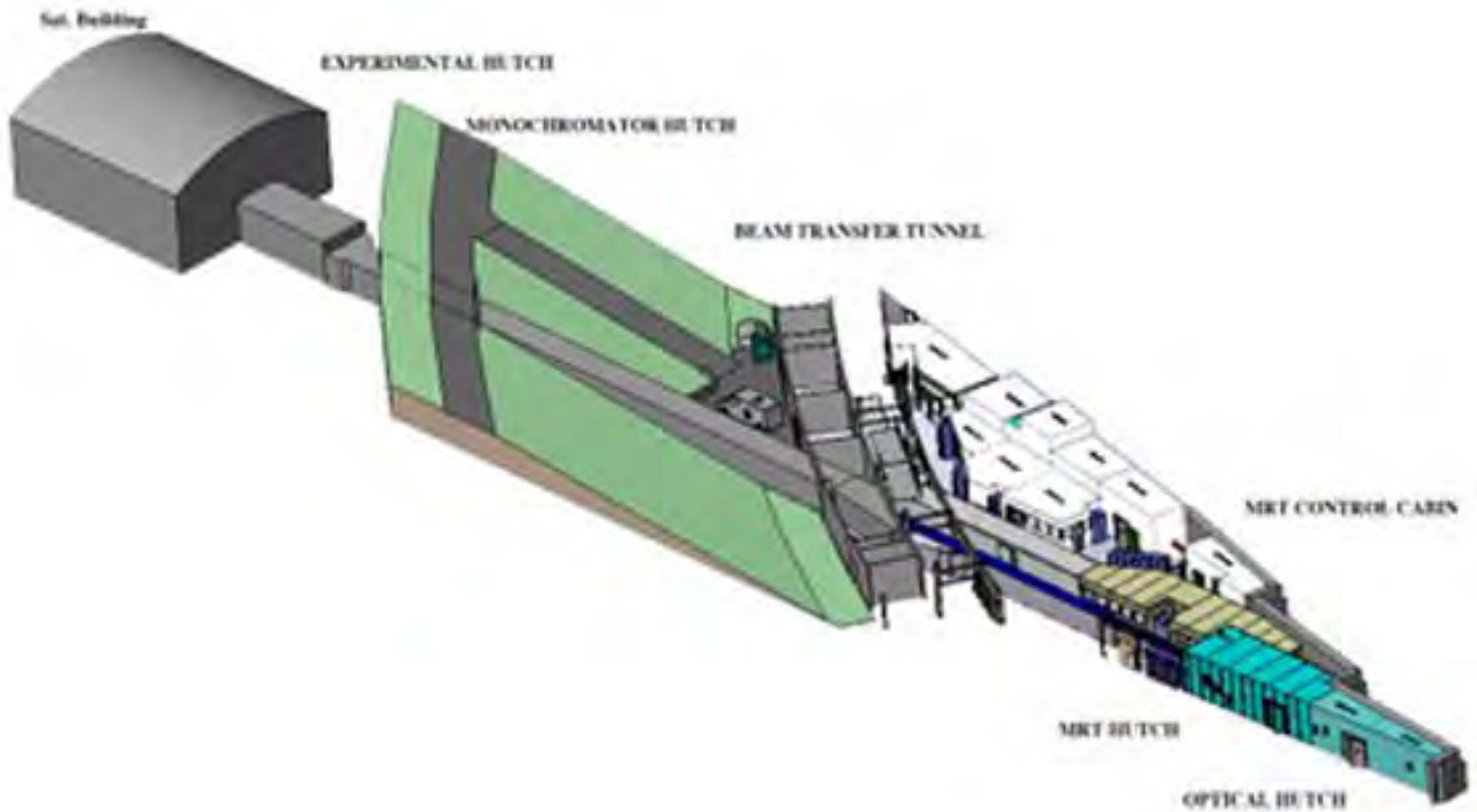
EXPERIMENTAL HUTCH
MONOCHROMATOR HUTCH
BEAM TRANSFER TUNNEL
MRT CONTROL CABIN
MRT HUTCH
OPTICAL HUTCH

Summary

- Fields of application for different type X-ray and gamma sources are different and they will be developed separately.

- At present we do not know the FS laser secondary beams applications completely. How to use the principal feature of secondary FS pulse radiation for biology or medicine purposes i?
- Micro beam radiation therapy ?

- In any case and first of all we have to solve fundamental problems:
- What is a wave packet of 10^{15} photons in the three dimension scale? Transversal dimension of the photon?

- FS photonuclear facilities future is more optimistic direction than plasma thermonuclear reactor?
- 20 years plus ….

So, for the FS laser driven X-ray and gamma source project we have still more questions than answers

Thank you for attention.

Acknowledgments to :

Ivanov K.A.[1], Shulyapov S.A.[1], Turinge A.A.[2], Brantov A.V.[3], Uryupina D.S[1]., Volkov R.V.[1], Rusakov A.V.[2], Djilkibaev R.M.[2], Bychenkov V.Yu[3]

1 - ILC MSU, 2 – INR RAS, 3 – FIAN

This work is supported by RFBR grant # 11-02-00286 a